Eidgenössische Technische Hochschule Zürich

Ecole polytechnique fédérale de Zurich
Politecnico federale di Zurigo
Swiss Federal Institute of Technology Zurich

Nonreflecting Boundary Conditions For Electromagnetic Scattering

M.J. Grote

Research Report No. 98-09
September 1998

Seminar für Angewandte Mathematik
Eidgenössische Technische Hochschule
CH-8092 Zürich
Switzerland

Nonreflecting Boundary Conditions For Electromagnetic Scattering

M.J. Grote

Seminar für Angewandte Mathematik
Eidgenössische Technische Hochschule
CH-8092 Zürich
Switzerland

Research Report No. 98-09 September 1998

Abstract

An exact nonreflecting boundary condition was derived previously for use with the time dependent Maxwell equations in three space dimensions[1]. Here it is shown how to combine that boundary condition with the variational formulation for use with the finite element method. The fundamental theory underlying the derivation of the exact boundary condition is reviewed. Numerical examples with the finite-difference time-domain method are presented which demonstrate the high accuracy and confirm the expected rate of convergence of the numerical method.

Keywords: Maxwell's equations, electromagnetic scattering, nonreflecting boundary conditions, absorbing boundary conditions, finite element method, finite difference method

AMS Subject Classification: 65M06, 65M60, 78-08, 78A40

1 Introduction

We consider electromagnetic scatterering in unbounded three-dimensional space. The scatterering region may contain obstacles, inhomogeneities, and nonlinearities. To treat it numerically we surround the region of interest by an artificial boundary $\mathcal{B}$, and we denote by Ω the computational domain inside $\mathcal{B}$. At $\mathcal{B}$ we impose an exact nonreflecting boundary condition upon the scattered field. This condition is local in time but nonlocal on $\mathcal{B}$. It is the extension to Maxwell's equations of the exact nonreflecting boundary condition which we have derived for the scalar wave equation [1]. We have shown [2] that it yields high accuracy in numerical computations.

Usually various approximate boundary conditions are used, which are local differential operators on $\mathcal{B}$. Examples are the Mur [3] and the Peterson [4] conditions, which are the generalizations to Maxwell's equations of the absorbing boundary conditions derived for the scalar wave equation by Engquist and Majda [5] and by Bayliss and Turkel [6]. A different approach has been to add an artificial absorbing layer outside $\mathcal{B}$, which is supposed to absorb outgoing waves [7]. Neither of these approaches leads to complete absorption of waves at all angles of incidence. To minimize the amount of reflection and to achieve very high accuracy, it is often necessary to move $\mathcal{B}$ far from the region of interest, or to use a thick absorbing layer. Both procedures are expensive in computer storage and execution time. Moreover, with limited memory it may not be possible to achieve a desired accuracy.

An exact nonreflecting boundary condition for the wave equation was proposed by Ting and Miksis [8]. It is based on a Kirchhoff integral representation of the solution outside $\mathcal{B}$, and it was generalized to Maxwell's equations by De Moerloose and De Zutter [9]. Since this boundary condition requires storing the solution at $\mathcal{B}$ for the amount of time it takes a wave to propagate across Ω, this approach is expensive in both storage and computer ressource requirements.

It is to avoid these difficulties that we have developed this new exact boundary condition for the special case when $\mathcal{B}$ is a sphere. The nonreflecting boundary condition is derived in section 2. In section 3 we shall show how to combine it with the finite difference method. Then in section 4, we shall derive alternative formulations, which are useful when the vector wave equation or the weak form of Maxwell's equations is used. In section 5, we shall discuss higher order boundary conditions, and finally in section 6, we shall present numerical results which demonstrate the high accuracy of our

boundary condition.

2 Derivation of the boundary conditions

We choose $\mathcal{B}$ to be a sphere of radius R. In $\mathcal{B}^{ext}$, the region outside $\mathcal{B}$, the medium is assumed to be linear, homogeneous, isotropic, of constant electric permittivity ε, of constant magnetic permeability μ, and of zero conductivity. In addition, we assume that at $t = 0$ the scattered field is confined to the computational domain Ω. In $\mathcal{B}^{ext}$ the electric field $\boldsymbol{E}$ and the magnetic field $\boldsymbol{H}$ satisfy Maxwell's equations

$$\nabla \times \boldsymbol{H} = \varepsilon \frac{\partial \boldsymbol{E}}{\partial t}, \qquad \nabla \times \boldsymbol{E} = -\mu \frac{\partial \boldsymbol{H}}{\partial t} \ . \tag{1}$$

Both $\boldsymbol{E}$ and $\boldsymbol{H}$ vanish at $t = 0$ in $\mathcal{B}^{ext}$, so $\nabla \cdot \boldsymbol{E} = \nabla \cdot \boldsymbol{H} = 0$ at $t = 0$. From (1) it follows that they remain solenoidal there for all time:

$$\nabla \cdot \boldsymbol{E} = \nabla \cdot \boldsymbol{H} = 0. \tag{2}$$

From (1) it also follows that both $\boldsymbol{E}$ and $\boldsymbol{H}$ satisfy the vector wave equation in $\mathcal{B}^{ext}$:

$$\frac{1}{c^2}\frac{\partial^2 \boldsymbol{E}}{\partial t^2} + \nabla \times \nabla \times \boldsymbol{E} = 0, \qquad \frac{1}{c^2}\frac{\partial^2 \boldsymbol{H}}{\partial t^2} + \nabla \times \nabla \times \boldsymbol{H} = 0. \tag{3}$$

Here $c = 1/\sqrt{\varepsilon\mu}$.

We introduce the polar coordinates r, ϑ, ϕ and the unit vectors $\hat{\boldsymbol{r}}$, $\hat{\boldsymbol{\vartheta}}$, $\hat{\boldsymbol{\phi}}$. Next, we let Y_{nm} denote the nm-th spherical harmonic

$$Y_{nm}(\vartheta, \phi) = \sqrt{\frac{(2n+1)(n-|m|)!}{4\pi(n+|m|)!}} P_n^{|m|}(\cos\vartheta) e^{im\phi}, \qquad n \geq 0, \ |m| \leq n. \tag{4}$$

The Y_{nm} are orthonormal with respect to the L_2 inner product on the *unit* sphere. If the problem considered is real, it is advantageous to use the real spherical harmonics, given by the real and imaginary parts of (4) with a modified normalization constant.

Following [10], p. 170, we let $\boldsymbol{U}_{nm}$ and $\boldsymbol{V}_{nm}$ denote the vector spherical harmonics

$$\boldsymbol{U}_{nm}(\vartheta, \phi) = \frac{r\nabla Y_{nm}}{\sqrt{n(n+1)}} = \frac{1}{\sqrt{n(n+1)}} \left[\frac{\partial Y_{nm}}{\partial \vartheta} \hat{\boldsymbol{\vartheta}} + \frac{1}{\sin\vartheta} \frac{\partial Y_{nm}}{\partial \phi} \hat{\boldsymbol{\phi}} \right], \tag{5}$$

$$\boldsymbol{V}_{nm}(\vartheta,\phi) = \hat{\boldsymbol{r}} \times \boldsymbol{U}_{nm} = \frac{1}{\sqrt{n(n+1)}} \left[\frac{-1}{\sin\vartheta} \frac{\partial Y_{nm}}{\partial \phi} \hat{\boldsymbol{\vartheta}} + \frac{\partial Y_{nm}}{\partial \vartheta} \hat{\boldsymbol{\phi}} \right]. \tag{6}$$

They form an orthonormal basis for the space of tangential L_2 fields on the unit sphere with respect to the L_2 inner product [10]. They also satisfy the following useful equations for any $f(r)$:

$$\nabla \times (f(r)\boldsymbol{V}_{nm}) = -\frac{\sqrt{n(n+1)}f(r)}{r} Y_{nm}\hat{\boldsymbol{r}} - \frac{1}{r}\frac{\partial (rf(r))}{\partial r}\boldsymbol{U}_{nm}, \tag{7}$$

$$\hat{\boldsymbol{r}} \times \nabla \times (f(r)\boldsymbol{V}_{nm}) = -\frac{1}{r}\frac{\partial (rf(r))}{\partial r}\boldsymbol{V}_{nm}. \tag{8}$$

To solve (1) in $\mathcal{B}^{ext}$, we decompose the electromagnetic field into transverse electric (TE) and transverse magnetic (TM) fields. The electric component of the TE multipole field of order (n,m) is given by

$$\boldsymbol{E}^{TE}_{nm}(r,\vartheta,\phi,t) = f_{nm}(r,t)\boldsymbol{V}_{nm}(\vartheta,\phi), \tag{9}$$

where f_{nm} satisfies

$$L_n[f_{nm}] \equiv \left(\frac{1}{c^2}\frac{\partial^2}{\partial t^2} - \frac{\partial^2}{\partial r^2} - \frac{2}{r}\frac{\partial}{\partial r} + \frac{n(n+1)}{r^2} \right) f_{nm} = 0. \tag{10}$$

The magnetic component of the TM multipole field of order (n,m) is given by

$$\boldsymbol{H}^{TM}_{nm}(r,\vartheta,\phi,t) = g_{nm}(r,t)\boldsymbol{V}_{nm}(\vartheta,\phi), \tag{11}$$

where $L_n[g_{nm}] = 0$.

The TE and TM solutions form a complete set of solutions of Maxwell's equations in a source-free region ([11], p. 746). Therefore the general electric and magnetic multipole field of order (n,m) are obtained by combining (9) with the electric field associated with (11), and combining (11) with the magnetic field associated with (9), respectively:

$$\boldsymbol{E}_{nm}(r,\vartheta,\phi,t) = f_{nm}(r,t)\boldsymbol{V}_{nm} + \frac{1}{\varepsilon}\nabla \times [\boldsymbol{V}_{nm}\int_0^t g_{nm}(r,s)\,ds], \tag{12}$$

$$\boldsymbol{H}_{nm}(r,\vartheta,\phi,t) = -\frac{1}{\mu}\nabla \times [\boldsymbol{V}_{nm}\int_0^t f_{nm}(r,s)\,ds] + g_{nm}(r,t)\boldsymbol{V}_{nm}. \tag{13}$$

In $\mathcal{B}^{ext}$, the total electromagnetic field is a superposition of multipole fields:

$$\boldsymbol{E} = \sum_{n\geq 1}\sum_{|m|\leq n} \boldsymbol{E}_{nm}, \qquad \boldsymbol{H} = \sum_{n\geq 1}\sum_{|m|\leq n} \boldsymbol{H}_{nm}. \tag{14}$$

By using (7) we see that the terms in (12) and (13) that involve $\nabla\times(\boldsymbol{V}_{nm}\ldots)$ are orthogonal to $\boldsymbol{V}_{nm}$. Thus from (14) we conclude that

$$f_{nm} = (\boldsymbol{E}, \boldsymbol{V}_{nm}), \qquad g_{nm} = (\boldsymbol{H}, \boldsymbol{V}_{nm}). \tag{15}$$

The inner product involves integration with respect to ϑ and ϕ on the sphere of radius r.

To obtain a boundary condition for $\boldsymbol{H}_{nm}$, we first apply $\hat{\boldsymbol{r}}\times\nabla\times$ to (13). We use (8) and the fact that $\boldsymbol{V}_{nm}\int_0^t f_{nm}$ is also a solution of (3) to get

$$\hat{\boldsymbol{r}}\times\nabla\times\boldsymbol{H}_{nm} = -\sqrt{\frac{\varepsilon}{\mu}}\frac{1}{c}\frac{\partial f_{nm}}{\partial t}\boldsymbol{U}_{nm} - \frac{1}{r}\frac{\partial(rg_{nm})}{\partial r}\boldsymbol{V}_{nm}. \tag{16}$$

Next we differentiate (13) with respect to t and simplify the result using (7). The tangential components of the resulting equation yield

$$\frac{1}{c}\frac{\partial \boldsymbol{H}_{nm}^{\tan}}{\partial t} = \sqrt{\frac{\varepsilon}{\mu}}\frac{1}{r}\frac{\partial(rf_{nm})}{\partial r}\boldsymbol{U}_{nm} + \frac{1}{c}\frac{\partial g_{nm}}{\partial t}\boldsymbol{V}_{nm}. \tag{17}$$

Now we subtract (17) from (16) to get

$$\begin{aligned}&\hat{\boldsymbol{r}}\times\nabla\times\boldsymbol{H}_{nm} - \frac{1}{c}\frac{\partial \boldsymbol{H}_{nm}^{\tan}}{\partial t} = \\ &-\sqrt{\frac{\varepsilon}{\mu}}\frac{1}{r}\left(\frac{\partial}{\partial r}+\frac{1}{c}\frac{\partial}{\partial t}\right)[rf_{nm}]\boldsymbol{U}_{nm} - \frac{1}{r}\left(\frac{\partial}{\partial r}+\frac{1}{c}\frac{\partial}{\partial t}\right)[rg_{nm}]\boldsymbol{V}_{nm}.\end{aligned} \tag{18}$$

Similarly from (12) we derive the equation

$$\begin{aligned}&\hat{\boldsymbol{r}}\times\nabla\times\boldsymbol{E}_{nm} - \frac{1}{c}\frac{\partial \boldsymbol{E}_{nm}^{\tan}}{\partial t} = \\ &-\frac{1}{r}\left(\frac{\partial}{\partial r}+\frac{1}{c}\frac{\partial}{\partial t}\right)[rf_{nm}]\boldsymbol{V}_{nm} + \sqrt{\frac{\mu}{\varepsilon}}\frac{1}{r}\left(\frac{\partial}{\partial r}+\frac{1}{c}\frac{\partial}{\partial t}\right)[rg_{nm}]\boldsymbol{U}_{nm}.\end{aligned} \tag{19}$$

Equations (18) and (19) cannot yet be used as boundary conditions because their right-hand sides involve radial derivatives of the unknown functions f_{nm} and g_{nm}. To eliminate these derivatives we note that f_{nm} and g_{nm} satisfy the differential equation (10), and that they both vanish at $t = 0$ for $r \geq R$. Equation (10) is the equation satisfied by the coefficient of Y_{nm} in the expansion of a solution of the scalar wave equation. Therefore at $r = R$,

f_{nm} satisfies the following boundary condition, which was derived in [1] for the wave equation, and used in [2]:

$$\left(\frac{\partial}{\partial r}+\frac{1}{c}\frac{\partial}{\partial t}\right)[rf_{nm}]=-\boldsymbol{d}_n\cdot\boldsymbol{\psi}^E_{nm}(t),\qquad r=R\ . \tag{20}$$

This is the nm-th component of (2.6) in [2] with $\boldsymbol{c}=\boldsymbol{d}$ and $\boldsymbol{z}=\boldsymbol{\psi}$. Here $\boldsymbol{d}_n$ and $\boldsymbol{\psi}^E_{nm}(t)$ are n-component vectors.

The vector function $\boldsymbol{\psi}^E_{nm}(t)=\{\psi^{E,j}_{nm}\}, j=1,\ldots,n$, satisfies the *linear first-order ordinary* differential equation

$$\frac{1}{c}\frac{d}{dt}\boldsymbol{\psi}^E_{nm}(t)=\boldsymbol{A}_n\boldsymbol{\psi}^E_{nm}(t)+f_{nm}(R,t)\boldsymbol{e}_n,\qquad \boldsymbol{\psi}^E_{nm}(0)=0. \tag{21}$$

Here $\boldsymbol{A}_n=\{A^{ij}_n\}$ is the constant $n\times n$ matrix

$$A^{ij}_n=\begin{cases}-n(n+1)/(2\,R^j) & \text{if } i=1,\\ (n+i)(n+1-i)/(2i) & \text{if } i=j+1,\\ 0 & \text{otherwise.}\end{cases} \tag{22}$$

The constant n-component vectors $\boldsymbol{d}_n=\{d^j_n\}$ and $\boldsymbol{e}_n=\{e^j_n\}$ are defined as

$$d^j_n \;=\; \frac{n(n+1)j}{2R^j},\qquad j=1,\ldots,n, \tag{23}$$

$$\boldsymbol{e}_n \;=\; [1,0,\ldots,0]^\top. \tag{24}$$

Since $L_n[g_{nm}]=0$, we also have

$$\left(\frac{\partial}{\partial r}+\frac{1}{c}\frac{\partial}{\partial t}\right)[rg_{nm}]=-\boldsymbol{d}_n\cdot\boldsymbol{\psi}^H_{nm}(t),\qquad r=R, \tag{25}$$

where the n-component vector function $\boldsymbol{\psi}^H_{nm}(t)$ satisfies the ordinary differential equation

$$\frac{1}{c}\frac{d}{dt}\boldsymbol{\psi}^H_{nm}(t)=\boldsymbol{A}_n\boldsymbol{\psi}^H_{nm}(t)+g_{nm}(R,t)\boldsymbol{e}_n,\qquad \boldsymbol{\psi}^H_{nm}(0)=0. \tag{26}$$

Now, we use (20) and (25) to eliminate the radial derivatives of f_{nm} and g_{nm} from (18) and (19). Thus we rewrite (18) and (19) at $r=R$ as

$$\hat{\boldsymbol{r}}\times\nabla\times\boldsymbol{H}_{nm}-\frac{1}{c}\frac{\partial\boldsymbol{H}^{\tan}_{nm}}{\partial t} \;=\; \sqrt{\frac{\varepsilon}{\mu}}\frac{1}{R}\boldsymbol{d}_n\cdot\boldsymbol{\psi}^E_{nm}(t)\boldsymbol{U}_{nm}$$

$$+ \quad \frac{1}{R}\boldsymbol{d}_n \cdot \boldsymbol{\psi}^H_{nm}(t)\boldsymbol{V}_{nm}, \qquad r = R, \tag{27}$$

$$\hat{\boldsymbol{r}} \times \nabla \times \boldsymbol{E}_{nm} - \frac{1}{c}\frac{\partial \boldsymbol{E}^{\tan}_{nm}}{\partial t} = \frac{1}{R}\boldsymbol{d}_n \cdot \boldsymbol{\psi}^E_{nm}(t)\boldsymbol{V}_{nm}$$

$$- \quad \sqrt{\frac{\mu}{\varepsilon}}\frac{1}{R}\boldsymbol{d}_n \cdot \boldsymbol{\psi}^H_{nm}(t)\boldsymbol{U}_{nm}, \qquad r = R. \tag{28}$$

Finally, we obtain the boundary condition at $r = R$ by summing over n and m in (27) and (28):

$$\hat{\boldsymbol{r}} \times \nabla \times \boldsymbol{H} - \frac{1}{c}\frac{\partial \boldsymbol{H}^{\tan}}{\partial t} = \sqrt{\frac{\varepsilon}{\mu}}\frac{1}{R}\sum_{n\geq 1}\sum_{|m|\leq n} \boldsymbol{d}_n \cdot \boldsymbol{\psi}^E_{nm}(t)\boldsymbol{U}_{nm}$$

$$+ \quad \frac{1}{R}\sum_{n\geq 1}\sum_{|m|\leq n} \boldsymbol{d}_n \cdot \boldsymbol{\psi}^H_{nm}(t)\boldsymbol{V}_{nm}, \qquad r = R, \tag{29}$$

$$\hat{\boldsymbol{r}} \times \nabla \times \boldsymbol{E} - \frac{1}{c}\frac{\partial \boldsymbol{E}^{\tan}}{\partial t} = \frac{1}{R}\sum_{n\geq 1}\sum_{|m|\leq n} \boldsymbol{d}_n \cdot \boldsymbol{\psi}^E_{nm}(t)\boldsymbol{V}_{nm}$$

$$- \quad \sqrt{\frac{\mu}{\varepsilon}}\frac{1}{R}\sum_{n\geq 1}\sum_{|m|\leq n} \boldsymbol{d}_n \cdot \boldsymbol{\psi}^H_{nm}(t)\boldsymbol{U}_{nm}, \qquad r = R. \tag{30}$$

The vector functions $\boldsymbol{\psi}^E_{nm}(t)$ and $\boldsymbol{\psi}^H_{nm}(t)$ in (29) and (30) satisfy the linear ordinary differential equations (21) and (26), which can be written as follows by using (15):

$$\frac{1}{c}\frac{d}{dt}\boldsymbol{\psi}^E_{nm}(t) = \boldsymbol{A}_n\boldsymbol{\psi}^E_{nm}(t) + \left(\boldsymbol{E}^{\tan}|_{r=R}\,, \boldsymbol{V}_{nm}\right)\boldsymbol{e}_n, \quad \boldsymbol{\psi}^E_{nm}(0) = 0. \tag{31}$$

$$\frac{1}{c}\frac{d}{dt}\boldsymbol{\psi}^H_{nm}(t) = \boldsymbol{A}_n\boldsymbol{\psi}^H_{nm}(t) + \left(\boldsymbol{H}^{\tan}|_{r=R}\,, \boldsymbol{V}_{nm}\right)\boldsymbol{e}_n, \quad \boldsymbol{\psi}^H_{nm}(0) = 0. \tag{32}$$

Each inner product in (31) and (32) involves two, not three, scalar inner products since $\boldsymbol{V}_{nm}$ is purely tangential. Equations (29) and (30) are the boundary conditions which we sought. They are exact and ensure that no spurious reflections occur at $\mathcal{B}$. They involve only first-order derivatives and can be incorporated easily into numerical methods.

The functions f_{nm} and g_{nm} satisfy the scalar wave equation and determine the electromagnetic field uniquely outside $\mathcal{B}$. It was shown in [2] that for smooth solutions of the scalar wave equation, imposing the exact boundary condition at $\mathcal{B}$ guarantees that the solution in Ω coincides with the restriction to Ω of the solution to the Cauchy problem in the unbounded domain.

Therefore for smooth data, the solution to the initial boundary value problem inside Ω with (29) or (30) imposed at $\mathcal{B}$, is unique and coincides with the restriction to Ω of the electromagnetic field in the unbounded domain. It is also well-posed with respect to perturbations in the initial conditions.

These boundary conditions do not require saving past values of $\boldsymbol{E}$ or $\boldsymbol{H}$. Instead they involve the two functions $\boldsymbol{\psi}^E_{nm}(t)$ and $\boldsymbol{\psi}^H_{nm}(t)$. The amount of memory needed to store them, about $4/3\,N^3$ scalar values, is negligible when compared to the storage required for $\boldsymbol{E}$ and $\boldsymbol{H}$. Most of the extra work involved in applying the boundary condition results from computing the inner products of $\boldsymbol{E}$ and $\boldsymbol{H}$ with $\boldsymbol{V}_{nm}$ in (31) and (32), and from computing the right-hand sides of (29) and (30).

To compute the Fourier components in (29) or (30), it is not necessary to compute $O(N^2)$ inner products over the entire sphere. Indeed, since the vector spherical harmonics $\boldsymbol{V}_{nm}$ separate in θ and ϕ, it is sufficient to compute $O(N)$ inner products with $\cos(m\phi)$ and $\sin(m\phi)$ over the sphere, and then to compute $O(N^2)$ *one-dimensional* inner products in θ over $[0,\pi]$. The same trick can be used to calculate the sums over n and m on the right of (29) and (30).

3 The finite difference method

We shall now show how the nonreflecting boundary condition fits into the finite difference time domain method (FDTD). First proposed by Yee [12], this popular method staggers both $\boldsymbol{E}$ and $\boldsymbol{H}$ in time and space, and thereby achieves second order accuracy using current values only. Due to the nature of the Yee scheme, the boundary condition is needed only for one of the two electromagnetic field components. We choose to apply it to $\boldsymbol{E}$. Thus $\boldsymbol{E}^{\tan}$ is known at $r = R - \Delta r$ and $r = R$, whereas $\boldsymbol{H}^{\tan}$ is known at $r = R - \Delta r/2$. The boundary condition is necessary to advance $\boldsymbol{E}^{\tan}$ at $r = R$, since Maxwell's equations (1) would require radial derivatives of $\boldsymbol{H}^{\tan}$, whose finite difference approximation involves unknown values of $\boldsymbol{H}^{\tan}$ outside $\mathcal{B}$. Thus we shall use (30) to advance $\boldsymbol{E}^{\tan}$ at $r = R$ from time t to time $t+\Delta t$. To do so, we apply (30) at $t = t + \Delta t/2$ and $r = R - \Delta r/2$, and approximate the first order derivatives on the left by centered finite differences ([13], section 3.7).

The right side of (30) involves infinite sums, which are truncated at a finite value N. It requires the values of $\boldsymbol{\psi}^E_{nm}(t)$ and $\boldsymbol{\psi}^H_{nm}(t)$ at $t = t + \Delta t/2$.

These are computed concurrently with the solution inside Ω, using the linear ordinary differential equations (31) and (32). The inner products in (31) and (32) are computed over the sphere $r = R - \Delta r/2$ using the fourth order Simpson rule. To solve (31) and (32) numerically, we opt for the trapezoidal rule ([14], sect. II.7), because the eigenvalues of the matrices $\boldsymbol{A}_n$ lie in the left half of the complex plane [2]. Since the trapezoidal rule is unconditionally stable, there is no restriction on the time-step in the integration of (31) and (32). The work required in solving the linear systems (31) and (32) is negligible, because the matrices $\boldsymbol{A}_n$ are very small and remain constant. The trapezoidal rule approximation of (31) is

$$\left(I - \frac{\Delta t}{2}\boldsymbol{A}_n\right)\boldsymbol{\psi}^E_{nm}(t_{k+1/2}) = \left(I + \frac{\Delta t}{2}\boldsymbol{A}_n\right)\boldsymbol{\psi}^E_{nm}(t_{k-1/2}) + \Delta t\left(\boldsymbol{E}^k\Big|_{R-\Delta r/2}, \boldsymbol{V}_{nm}\right)\boldsymbol{e}_n, \tag{33}$$

where $\boldsymbol{E}^k$ at $r = R - \Delta r/2$ is the average of $\boldsymbol{E}^k$ at $r = R - \Delta r$ and $r = R$. The trapezoidal rule approximation of (32) is

$$\begin{aligned}\left(I - \frac{\Delta t}{2}\boldsymbol{A}_n\right)\boldsymbol{\psi}^H_{nm}(t_{k+1/2}) &= \left(I + \frac{\Delta t}{2}\boldsymbol{A}_n\right)\boldsymbol{\psi}^H_{nm}(t_{k-1/2}) \\ &+ \frac{\Delta t}{2}\left(\boldsymbol{H}^{k-1/2}\Big|_{R-\Delta r/2} + \boldsymbol{H}^{k+1/2}\Big|_{R-\Delta r/2}, \boldsymbol{V}_{nm}\right)\boldsymbol{e}_n.\end{aligned} \tag{34}$$

The complete algorithm proceeds as follows:

0. Initialize $\boldsymbol{E}$ at $t = 0$ and $\boldsymbol{H}$ at $t = \Delta t/2$, and set $\boldsymbol{\psi}^E_{nm} = 0$ and $\boldsymbol{\psi}^H_{nm} = 0$ at $t = \Delta t/2$.

1. Compute $\boldsymbol{E}$ at $t_k = t_{k-1} + \Delta t$ at all inner points of Ω using (1).

2. Compute $\boldsymbol{E}^{\tan}$ at t_k and $r = R$ using (30) applied at $r = R - \Delta r/2$ and $t_{k-1/2} = t_{k-1} + \Delta t/2$.

3. Compute $\boldsymbol{H}$ at $t_{k+1/2}$ using (1).

4. Compute $\boldsymbol{\psi}^E_{nm}$ and $\boldsymbol{\psi}^H_{nm}$ at $t_{k+1/2}$ using (33) and (34), respectively, and return to 1.

Although the artificial boundary must be spherical, the boundary condition is not tied to any coordinate system, and the grid used inside Ω can be arbitrary. See [15] for how to fit a Cartesian mesh to curvilinear coordinates, or [16] for a structured spherical mesh without singularities.

4 Alternative formulations

We shall now show how to reduce the work involved in forming the inner products in (31)–(32). This slight modification will also render the boundary condition particularly useful when the problem is formulated in terms of $\boldsymbol{E}$ (or $\boldsymbol{H}$) only and the vector wave equation (2) is used in Ω. Next, we shall present an alternative formulation of the boundary condition, which fits naturally into the weak formulation of the problem, and therefore is ideally suited for the finite element method.

The work involved in forming the inner products with $\boldsymbol{E}^{\tan}$ and $\boldsymbol{H}^{\tan}$ in (31)–(32) can be reduced. Indeed, if we compute $\hat{\boldsymbol{r}} \cdot \partial_t \boldsymbol{E}_{nm}$ in (12) and use (7), we see that

$$\hat{\boldsymbol{r}} \cdot \frac{\partial \boldsymbol{E}_{nm}}{\partial t} = -\frac{\sqrt{n(n+1)}}{\varepsilon R} g_{nm} Y_{nm}, \quad r = R. \tag{35}$$

By taking the inner product of (35) with Y_{nm} we get

$$g_{nm} = -\frac{\varepsilon R}{\sqrt{n(n+1)}} (\hat{\boldsymbol{r}} \cdot \frac{\partial \boldsymbol{E}}{\partial t}, Y_{nm}), \qquad r = R. \tag{36}$$

Therefore, we can compute g_{nm} with one scalar inner product. The time derivative in (36) can be replaced by *tangential* spatial derivatives by using (1) to yield

$$g_{nm} = -\frac{R}{\sqrt{n(n+1)}} (\hat{\boldsymbol{r}} \cdot \nabla \times \boldsymbol{H}, Y_{nm}), \qquad r = R. \tag{37}$$

Similarly,

$$f_{nm} = \frac{\mu R}{\sqrt{n(n+1)}} (\hat{\boldsymbol{r}} \cdot \frac{\partial \boldsymbol{H}}{\partial t}, Y_{nm}), \qquad r = R, \tag{38}$$

$$= -\frac{R}{\sqrt{n(n+1)}} (\hat{\boldsymbol{r}} \cdot \nabla \times \boldsymbol{E}, Y_{nm}), \qquad r = R. \tag{39}$$

Equations (36) and (39) are particularly useful when the vector wave equation is used inside Ω and the problem is written in terms of $\boldsymbol{E}$ (or $\boldsymbol{H}$) only. Then the boundary condition (30) can be used, with $(\boldsymbol{H}, \boldsymbol{V}_{nm})$ in (32)

replaced by the right side of (36). Thus applying the boundary condition at $\mathcal{B}$ involves only tangential derivatives of $\boldsymbol{E}$.

The boundary conditions (29) and (30) fit naturally into finite difference methods. We shall now show how they can be reformulated easily to accomodate finite element methods. To derive the weak form of Maxwell's equations, both equations (1) are multiplied by test functions and integrated over Ω. Integration by parts then introduces terms of the form $\hat{\boldsymbol{r}} \times \boldsymbol{E}$ or $\hat{\boldsymbol{r}} \times \boldsymbol{H}$ over $\mathcal{B}$ (see [17], [18]), which we shall now express in terms of known quantities.

We begin by introducing

$$\boldsymbol{\Psi}^E_{nm}(t) = \int_0^t \boldsymbol{\psi}^E_{nm}(s)\, ds, \qquad \boldsymbol{\Psi}^H_{nm}(t) = \int_0^t \boldsymbol{\psi}^H_{nm}(s)\, ds. \tag{40}$$

Therefore, $\boldsymbol{\Psi}^E_{nm}$ and $\boldsymbol{\Psi}^H_{nm}$ satisfy the same ordinary differential equations as $\boldsymbol{\psi}^E_{nm}$ and $\boldsymbol{\psi}^H_{nm}$, but with f_{nm} and g_{nm} replaced by their time integrals. By integrating (36) and (39) in time, we conclude that $\boldsymbol{\Psi}^E_{nm}$ is the solution of

$$\frac{1}{c}\frac{d}{dt}\boldsymbol{\Psi}^E_{nm}(t) = \boldsymbol{A}_n \boldsymbol{\Psi}^E_{nm}(t) + \frac{\mu R}{\sqrt{n(n+1)}}(\hat{\boldsymbol{r}} \cdot \boldsymbol{H}|_{r=R}, Y_{nm})\, \boldsymbol{e}_n, \qquad \boldsymbol{\Psi}^E_{nm}(0) = 0, \tag{41}$$

and that $\boldsymbol{\Psi}^H_{nm}$ is the solution of

$$\frac{1}{c}\frac{d}{dt}\boldsymbol{\Psi}^H_{nm}(t) = \boldsymbol{A}_n \boldsymbol{\Psi}^H_{nm}(t) - \frac{\varepsilon R}{\sqrt{n(n+1)}}(\hat{\boldsymbol{r}} \cdot \boldsymbol{E}|_{r=R}, Y_{nm})\, \boldsymbol{e}_n, \qquad \boldsymbol{\Psi}^H_{nm}(0) = 0. \tag{42}$$

We note that the inner products in (41) and (42) involve only scalar inner products with the radial components of $\boldsymbol{E}$ and $\boldsymbol{H}$. Next, we integrate (29) and (30) with respect to time. The right sides remain the same, with $\boldsymbol{\psi}^E_{nm}$ and $\boldsymbol{\psi}^H_{nm}$ replaced by $\boldsymbol{\Psi}^E_{nm}$ and $\boldsymbol{\Psi}^H_{nm}$. The left sides can be reformulated easily using (1), which leads to the alternative formulation of the nonreflecting boundary condition at $r = R$:

$$\begin{aligned} \varepsilon \hat{\boldsymbol{r}} \times \boldsymbol{E} - \frac{1}{c}\boldsymbol{H}^{\tan} &= \sqrt{\frac{\varepsilon}{\mu}}\frac{1}{R}\sum_{n\geq 1}\sum_{|m|\leq n} \boldsymbol{d}_n \cdot \boldsymbol{\Psi}^E_{nm}(t)\boldsymbol{U}_{nm} \\ &+ \frac{1}{R}\sum_{n\geq 1}\sum_{|m|\leq n} \boldsymbol{d}_n \cdot \boldsymbol{\Psi}^H_{nm}(t)\boldsymbol{V}_{nm}, \qquad r = R, \end{aligned} \tag{43}$$

$$\begin{aligned} \mu \hat{\boldsymbol{r}} \times \boldsymbol{H} + \frac{1}{c}\boldsymbol{E}^{\tan} &= -\frac{1}{R}\sum_{n\geq 1}\sum_{|m|\leq n} \boldsymbol{d}_n \cdot \boldsymbol{\Psi}^E_{nm}(t)\boldsymbol{V}_{nm} \\ &+ \sqrt{\frac{\mu}{\varepsilon}}\frac{1}{R}\sum_{n\geq 1}\sum_{|m|\leq n} \boldsymbol{d}_n \cdot \boldsymbol{\Psi}^H_{nm}(t)\boldsymbol{U}_{nm}, \qquad r = R. \end{aligned} \tag{44}$$

Either (43) or (44) can be used in the weak formulation of the problem inside Ω. Since they do not involve any derivatives of $\boldsymbol{E}$ or $\boldsymbol{H}$, they are particularly easy to combine with a numerical method. When the method of lines is used, the vector of unknowns involves the values of $\boldsymbol{E}$ and $\boldsymbol{H}$ at the interior nodes, together with the unknown functions $\boldsymbol{\Psi}^E_{nm}(t)$ and $\boldsymbol{\Psi}^H_{nm}(t)$, which are advanced concurrently using (41) and (42). It is quite remarkable that the two scalar quantities $\hat{\boldsymbol{r}}\cdot\boldsymbol{E}$ and $\hat{\boldsymbol{r}}\cdot\boldsymbol{H}$ suffice to impose the nonreflecting boundary condition.

5 Higher order boundary conditions

In practice, the infinite sums in (29) and (30) must be truncated at some finite value N. For the modes $n > N$, the truncated boundary condition for $\boldsymbol{H}$ reduces to

$$\hat{\boldsymbol{r}} \times \nabla \times \boldsymbol{H} - \frac{1}{c}\frac{\partial \boldsymbol{H}^{\tan}}{\partial t} = 0. \tag{45}$$

This is the time-dependent counterpart of the first-order approximate boundary condition derived by Peterson [4], which annihilates the leading term in the large distance expansion of the electromagnetic field [19]. The truncation at N introduces an error $O(R^{-3})$ in modes with $n > N$. To reduce that error, without affecting the modes $n \le N$, we transform the second-order Peterson condition [4] to the time domain to obtain

$$\left\{\hat{\boldsymbol{r}} \times (\nabla\times\,) - \frac{1}{c}\frac{\partial}{\partial t} - \frac{2}{r}\right\}\left\{\hat{\boldsymbol{r}} \times \nabla \times \boldsymbol{H} - \frac{1}{c}\frac{\partial \boldsymbol{H}^{\tan}}{\partial t}\right\} = 0, \qquad r = R. \tag{46}$$

The error in (46) is $O(R^{-5})$, which is smaller than the error $O(R^{-3})$ in (45) for $R > 1$.

To take advantage of this smaller error, we apply the operator $(\hat{\boldsymbol{r}}\times(\nabla\times\,) - c^{-1}\partial_t - 2/r)$ to both sides of (29) and (30). The resulting boundary conditions are still exact, but when truncated at $n = N$ they yield (46) for the modes with $n > N$, with error $O(R^{-5})$. We shall carry out the calculations for the component $\boldsymbol{H}_{nm}$, which satisfies (18). To do so we derive the following formula, similar to (8), which holds for any $f(r)$:

$$\hat{\boldsymbol{r}} \times \nabla \times (f(r)\boldsymbol{U}_{nm}) = -\frac{1}{r}\frac{\partial(rf(r))}{\partial r}\boldsymbol{U}_{nm}. \tag{47}$$

By using (8) and (47) we obtain from (18)

$$\left\{\hat{\boldsymbol{r}}\times(\nabla\times)-\frac{1}{c}\frac{\partial}{\partial t}-\frac{2}{r}\right\}\left\{\hat{\boldsymbol{r}}\times\nabla\times\boldsymbol{H}_{nm}-\frac{1}{c}\frac{\partial\boldsymbol{H}_{nm}^{\tan}}{\partial t}\right\}=$$
$$\sqrt{\frac{\varepsilon}{\mu}}\frac{1}{r}\left(\frac{\partial}{\partial r}+\frac{1}{c}\frac{\partial}{\partial t}+\frac{2}{r}\right)\left(\frac{\partial}{\partial r}+\frac{1}{c}\frac{\partial}{\partial t}\right)[rf_{nm}]\boldsymbol{U}_{nm}$$
$$+\frac{1}{r}\left(\frac{\partial}{\partial r}+\frac{1}{c}\frac{\partial}{\partial t}+\frac{2}{r}\right)\left(\frac{\partial}{\partial r}+\frac{1}{c}\frac{\partial}{\partial t}\right)[rg_{nm}]\boldsymbol{V}_{nm}. \tag{48}$$

In ([2], sect. 5) it was shown that the exact second-order boundary condition for $f_{nm}(r,t)$ is

$$\left(\frac{\partial}{\partial r}+\frac{1}{c}\frac{\partial}{\partial t}+\frac{2}{r}\right)\left(\frac{\partial}{\partial r}+\frac{1}{c}\frac{\partial}{\partial t}\right)[rf_{nm}]=\tilde{\boldsymbol{d}}_n\cdot\boldsymbol{\psi}_{nm}^E(t),\qquad r=R, \tag{49}$$

where the vector functions $\boldsymbol{\psi}_{nm}^E(t)$ satisfy (21), and the constant vectors $\tilde{\boldsymbol{d}}_n=\{\tilde{d}_n^j\}$ are defined by

$$\tilde{d}_n^j=\frac{n(n+1)j(j-1)}{2R^j},\qquad j=1,\ldots,n. \tag{50}$$

We note that $\tilde{d}_1^1=0$, and hence that the terms with $n=1$ in the sums vanish. Therefore the second-order absorbing boundary condition (46) is exact for the multipoles with $n=1$.

We use (49) in (48), set $r=R$, and finally sum over n and m to obtain the exact nonreflecting boundary condition. The exact second-order boundary condition for the magnetic field at $r=R$ is

$$\left\{\hat{\boldsymbol{r}}\times(\nabla\times)-\frac{1}{c}\frac{\partial}{\partial t}-\frac{2}{R}\right\}\left\{\hat{\boldsymbol{r}}\times\nabla\times\boldsymbol{H}-\frac{1}{c}\frac{\partial\boldsymbol{H}^{\tan}}{\partial t}\right\}$$
$$=\sqrt{\frac{\varepsilon}{\mu}}\frac{1}{R^2}\sum_{n\geq2}\sum_{|m|\leq n}\tilde{\boldsymbol{d}}_n\cdot\boldsymbol{\psi}_{nm}^E(t)\boldsymbol{U}_{nm}+\frac{1}{R^2}\sum_{n\geq2}\sum_{|m|\leq n}\tilde{\boldsymbol{d}}_n\cdot\boldsymbol{\psi}_{nm}^H(t)\boldsymbol{V}_{nm}. \tag{51}$$

The exact second-order boundary condition for the electric field at $r=R$ is

$$\left\{\hat{\boldsymbol{r}}\times(\nabla\times)-\frac{1}{c}\frac{\partial}{\partial t}-\frac{2}{R}\right\}\left\{\hat{\boldsymbol{r}}\times\nabla\times\boldsymbol{E}-\frac{1}{c}\frac{\partial\boldsymbol{E}^{\tan}}{\partial t}\right\}$$
$$=\frac{1}{R^2}\sum_{n\geq2}\sum_{|m|\leq n}\tilde{\boldsymbol{d}}_n\cdot\boldsymbol{\psi}_{nm}^E(t)\boldsymbol{V}_{nm}-\sqrt{\frac{\mu}{\varepsilon}}\frac{1}{R^2}\sum_{n\geq2}\sum_{|m|\leq n}\tilde{\boldsymbol{d}}_n\cdot\boldsymbol{\psi}_{nm}^H(t)\boldsymbol{U}_{nm}. \tag{52}$$

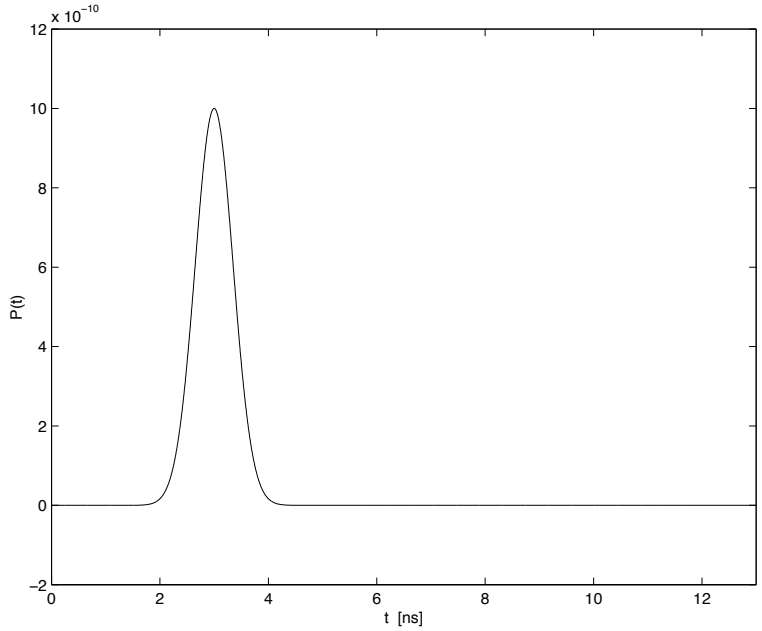

Figure 1: The time dependence $P(t)$ of the dipole source.

Here the vector functions $\boldsymbol{\psi}_{nm}^{E}(t)$ and $\boldsymbol{\psi}_{nm}^{H}(t)$ satisfy the same ordinary differential equations (31) and (32). The constant vectors $\tilde{\boldsymbol{d}}_n$ are given by (50), $\boldsymbol{e}_n$ by (24), and the constant matrices $\boldsymbol{A}_n$ by (22).

The same procedure can be adapted easily to accomodate modifications of (46), which may possess certain practical advantages [20]. If the radius of $\mathcal{B}$ and the temporal frequency remain fixed, the error introduced at $\mathcal{B}$ by imposing (46) on the multipole $\boldsymbol{H}_{nm}$ increases with increasing n [20].

6 Numerical results

We shall now combine the finite difference method with the nonreflecting boundary condition, as described in section 3, and apply it to a model problem for which the exact solution is known.

We consider an off-centered radiating electric dipole located at $S = (0, 0, z_0)$, $z_0 > 0$, at distance z_0 from the origin. The dipole is aligned along z, so that its moment points along the positive z-axis. Its time dependence,

shown in figure 1, is a Gaussian pulse centered at $t = t_0$:

$$P(t) = \begin{cases} 0 & t < 0, \\ \alpha e^{-(t-t_0)^2/\sigma^2} & 0 \le t \le 2t_0, \\ 0 & t > 2t_0. \end{cases} \tag{53}$$

We set $\alpha = 10^{-9}$ and choose σ so that $P(t)$ is equal to machine precision at $t = 0$ and $t = 2t_0$.

Since this problem is symmetric about the z-axis, the electromagnetic field has only three nonvanishing components: $\boldsymbol{E}(r, \theta, t) = E^r \hat{\boldsymbol{r}} + E^\theta \hat{\boldsymbol{\vartheta}}$, and $\boldsymbol{H}(r, \theta, t) = H^\phi \hat{\boldsymbol{\phi}}$. Furthermore, the exact solution can be found in ([22], p. 152). We impose the tangential component E^θ of the exact solution as a boundary condition at $r = r_0$, and calculate its propagation outwards up to the artificial boundary $r = R$. Because of the inherent symmetry, the computational domain Ω can be reduced to the two-dimensional region $r_0 \le r \le R$, $0 \le \theta \le \pi$, shown in figure 2. Inside Ω we use polar coordinates and a uniform mesh in r and θ. The Yee algorithm in polar coordinates is described in [21] or ([13], pp. 378–381). We set $r_0 = 0.5$ [m], $R = 1$ [m], $z_0 = 0.4$ [m], $c = 2.998 \times 10^8$ [m/s], and $t_0 = 3$ [ns].

We shall compare the numerical solution using (30), where the sums are truncated at N, with that obtained using the first order condition (45). We denote the former by NBC(N), where N indicates the upper limit in the sums, and the latter by P1 to acknowledge [4]. We recall that P1 is identical to NBC(0). The boundary condition (30) is implemented as described in section 3, albeit due to the radial symmetry, $\boldsymbol{\psi}^E_{nm}(t)$ is identically zero.

In figure 3, we check the accuracy of our numerical method. The maximal error in the L_2-norm over the time interval $[0, 15]$ nanoseconds is shown versus the mesh parameter $h = \Delta r$, for the following sequence of meshes: 20×120, 30×180, 40×240, 60×360, and 80×480. We observe the expected second order convergence of the the full scheme using NBC(20) as the mesh is refined. This indicates that setting $N = 20$ ensures that the error introduced at the artificial boundary is smaller than that of the numerical scheme. However, the error in the numerical solution obtained with P1 does not decrease as the mesh is refined, indicating that the error introduced by using P1 dominates the computation. Indeed, the numerical solution does not converge to the solution of the original problem, but instead converges to the solution of a different problem with P1 imposed at $\mathcal{B}$. When implemented numerically, N can be chosen large enough to reduce the error introduced at $\mathcal{B}$ below the

discretization error of the numerical method inside Ω, without moving the artificial boundary farther away from the scatterer.

Next, we shall compare the numerical solutions, obtained using P1 and NBC(20), with the exact solution at three different locations well inside Ω at $r = 0.75$ [m] : Q_1 ($\theta = 45°$), Q_2 ($\theta = 135°$), and Q_3 ($\theta = 170°$). The inner and outer radii remain at their current locations $r_0 = 0.5$ [m] and $R = 1$ [m], and we choose a 60×360 mesh inside Ω.

In figure 4, the ϕ-component of the magnetic field is shown at the first location Q_1. The numerical solution obtained with NBC(20) is hardly distinguishable from the exact solution. While the relative error due to the P1 boundary condition is only a few percent, this seemingly accurate behavior is deceptive.

Indeed these *locally* small reflections travel back into the computational domain, and contaminate the solution everywhere inside Ω, in particular in regions where the solution is of much lesser magnitude. To demonstrate this point, we select the next location farther from the source at Q_2, where the electromagnetic field is much weaker. The ϕ-component of the magnetic field at Q_2 is shown in figure 5, and again it agrees completely with the numerical solution obtained using NBC(20). The solution obtained using P1 agrees with the exact solution for a finite time. It then diverges from it, as the spurious reflection due to the imposition of P1 reaches this location.

This effect is even more dramatic if we choose a location close to the south pole at Q_3. In figure 6, the ϕ-component of the magnetic field is shown at Q_3. Here the spurious reflection due to the P1 boundary condition is *larger than the original signal*. The solution obtained using NBC(20) agrees well with the exact solution.

Finally, we set $R = 0.6$ [m] to study the performance of the boundary conditions as the outer boundary is moved closer to the inner one. The mesh size remains identical, so that the mesh has 12×360 points. In figure 7, the r-component of the electric field is shown below the south pole of the inner sphere at the severe test location $\theta = 180°$ and $r = 0.55$ [m]. Again, the numerical solution obtained using NBC(20) agrees with the exact solution; this demonstrates the robustness of the exact boundary condition with respect to the location of the artificial boundary. The numerical solution obtained with P1 agrees with the exact solution for a short time. It then strongly overshoots, oscillates a few times, and slowly starts to approach zero. This suggests that using the exact nonreflecting boundary condition may be

useful even in calculations where the transient behavior is of no interest, since the numerical solution may reach the final steady-state much faster.

7 Conclusion

We have derived an exact boundary condition for the time-dependent Maxwell equations in three space dimensions. It holds at the surface of a sphere and is local in time. It is given by (29) and (30), and fits naturally into standard finite difference methods. An alternative formulation, more suitable for finite element methods, is given by (43) and (44). Both boundary conditions require little extra storage and computer time, and can reduce the error introduced by the artificial boundary below the discretization error due to the numerical method, regardless of the radius of the outer boundary.

References

[1] M. J. Grote and J. B. Keller, *Exact nonreflecting boundary conditions for the time dependent wave equation*, SIAM J. Appl. Math., April 95.

[2] M. J. Grote and J. B. Keller, *Nonreflecting boundary conditions for time dependent scattering*, J. Comput. Phys., in press.

[3] G. Mur, *Absorbing boundary conditions for the finite-difference approximation of the time-domain electromagnetic-field equations*, IEEE Trans. Electromagn. Compat., Vol. EMC–23, No. 4, Novmber 1981.

[4] A. F. Peterson, *Absorbing boundary conditions for the vector wave equation*, Microwave and Optical Techn. Letters, vol. 1, No. 2, April 1988.

[5] B. Engquist and A. Majda, *Absorbing boundary conditions for the numerical simulation of waves*, Math. Comp., Vol. 31, pp. 629–651, July 1977.

[6] A. Bayliss and E. Turkel, *Radiation boundary conditions for wave-like equations*, Comm. Pure Appl. Math., vol. 33, pp. 707–725, 1980.

[7] J.-P. Bérenger, *A perfectly matched layer for the absorbtion of electromagnetic waves*, J. Comput. Phys. 114, pp. 185–200, 1994.

[8] L. Ting and M. J. Miksis, *Exact boundary conditions for scattering problems*, J. Acoust. Soc. Amer., vol. 80, pp. 1825–1827.

[9] J. De Moerloose and D. De Zutter, *Surface integral representation radiation boundary condition for the FDTD method*, IEEE Trans. Antenn. Propag., vol. 41, no. 7, July 1993, pp. 890–895.

[10] D. Colton and R. Kress, *Inverse Acoustic and Electromagnetic Scattering Theory*, Springer Verlag, 1992.

[11] J. D. Jackson, *Classical Electrodynamics*, 2nd edition, John Wiley & Sons, 1975.

[12] K. S. Yee, *Numerical solution of initial boundary value problems involving Maxwell's equations in isotropic media*, IEEE Trans. Antennas Propag., AP–14, No. 3, pp. 302–307, May 1966.

[13] K. S. Kunz and R. J. Luebbers, *Finite Difference Time Domain Methods for Electromagnetics*, CRC Press, 1993.

[14] E. Hairer, S. P. Nørsett, G. Wanner, *Solving Ordinary Differential Equations I*, Springer Verlag, 1987.

[15] A. Taflove and K. R. Umashankar, *The finite-difference time-domain method for numerical modeling of electromagnetic wave interactions*, Electromagnetics, Vol. 10, pp. 105–126, 1990.

[16] C. Ronchi, R. Iacono, P. S. Paolucci, *The "cubed sphere": a new method for the solution of partial differential equations in spherical geometry*, J. Comput. Phys., vol. 124, pp. 93–114, 1996.

[17] R. L. Lee and N. K. Madsen, *A mixed finite element formulation for Maxwell's equations in the time domain*, J. Comput. Phys., vol. 88, pp. 284–304, 1990.

[18] P. Monk, *A comparison of three mixed methods for the time-dependent Maxwell's equations*, SIAM J. Sci. Stat. Comput., Vol. 13, No. 5, pp. 1097–1122, September 1992.

[19] C. H. Wilcox, *An expansion theorem for electromagnetic fields*, Comm. Pure Appl. Math., Vol. 9, pp. 115–134, 1956.

[20] A. F. Peterson, *Absorbing boundary conditions for the vector wave equation*, IEEE Trans. Antenn. Propag., Vol. 40, No. 3, pp. 351–355, March 1992.

[21] R. Holland, *THREDS: A finite-difference time-domain EMP code in 3D spherical coordinates*, IEEE Trans. Nucl. Science, Vol. NS–30, No. 6, December, 1983.

[22] D. S. Jones, *The Theory of Electromagnetism*, Pergamon Press, New York, Macmillan, 1964.

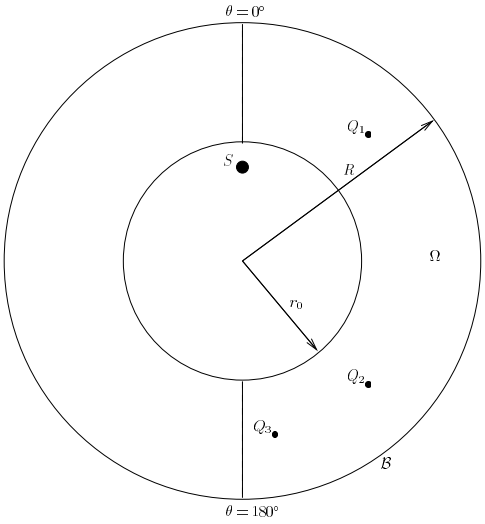

Figure 2: The computational domain Ω is shown drawn to scale, with $r_0 = 0.5$ [m] and $R = 1$ [m]. The dipole source is located at $S = (0, 0, z_0)$, with $z_0 = 0.4$ [m].

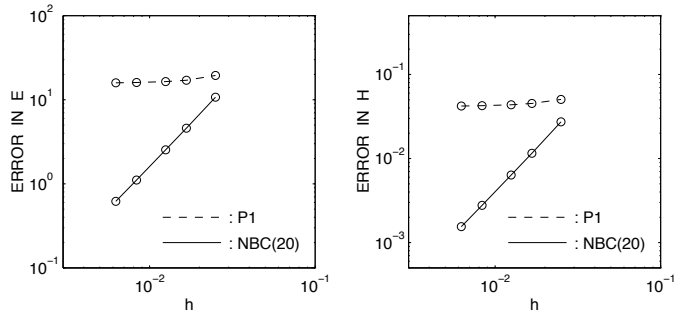

Figure 3: The maximal error in the L_2 norm over the time interval $[0, 15]$ nanoseconds is shown versus the mesh parameter $h = \Delta r$: $\boldsymbol{E}^h$ (left) and $\boldsymbol{H}^h$ (right).

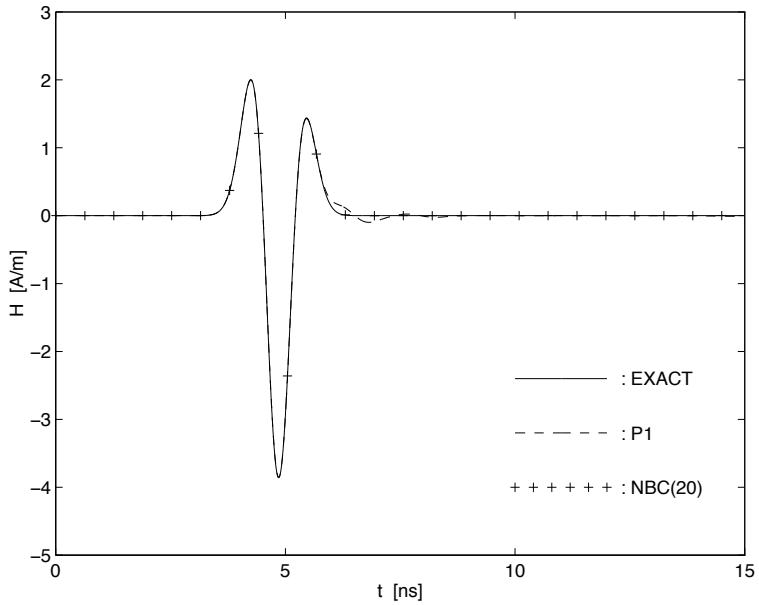

Figure 4: The numerical solutions for H^ϕ, computed using the boundary conditions P1 and NBC(20), are compared with the exact solution at Q_1.

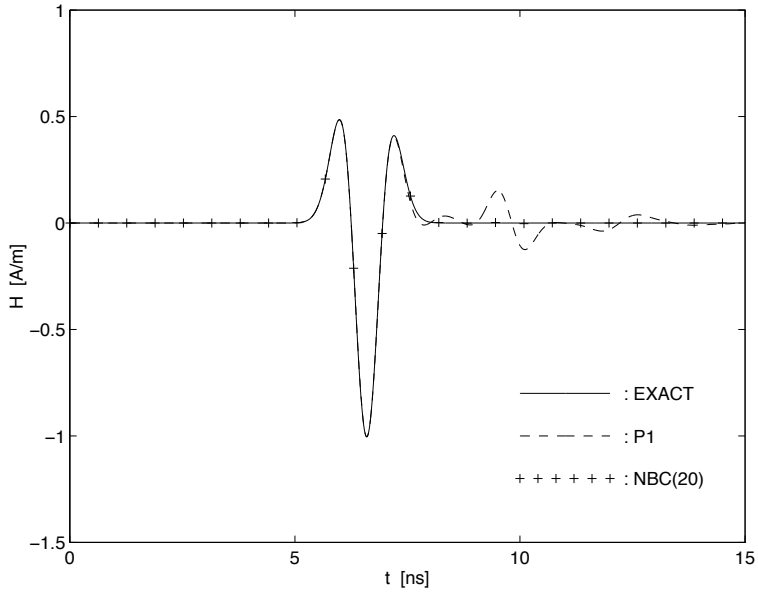

Figure 5: The numerical solutions for H^{ϕ}, computed using the boundary conditions P1 and NBC(20), are compared with the exact solution at Q_2.

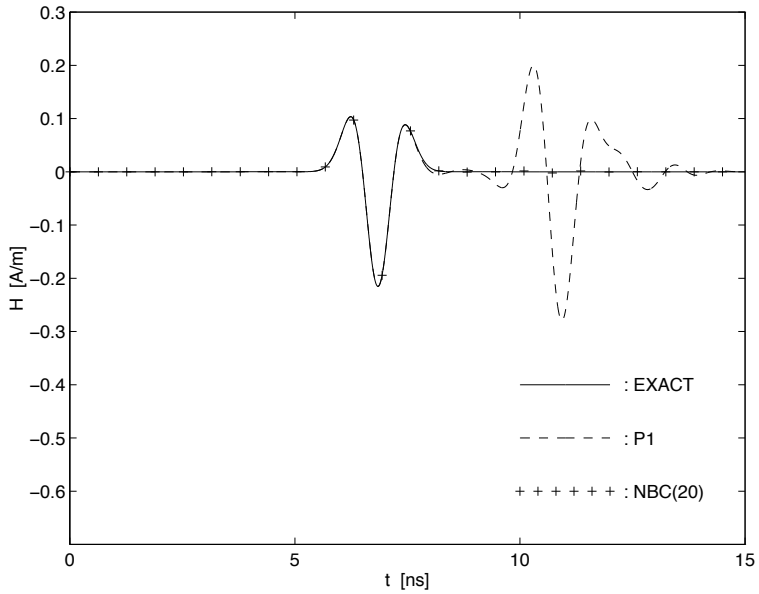

Figure 6: The numerical solutions for H^{ϕ}, computed using the boundary conditions P1 and NCB(20), are compared with the exact solution at Q_3.

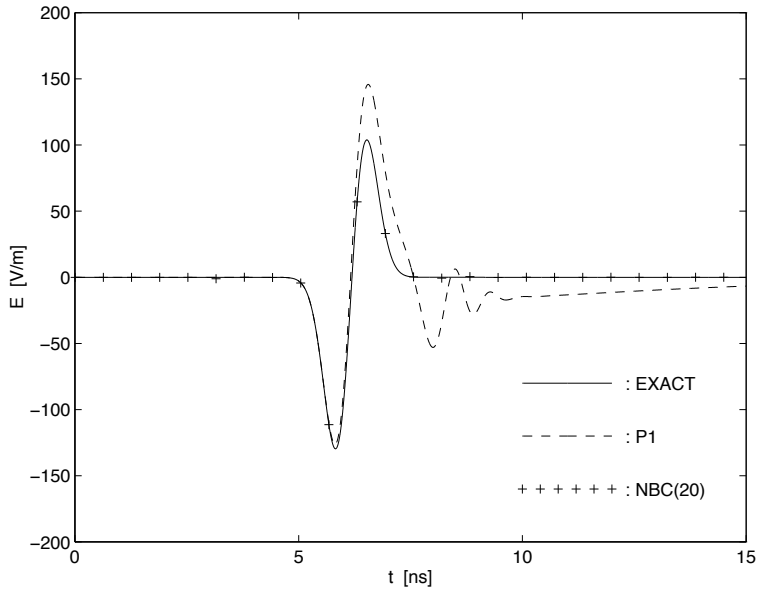

Figure 7: The numerical solutions for E^r, computed using the boundary conditions P1 and NCB(20) at $R = 0.6$ [m], are compared with the exact solution at $r = 0.55$ [m], $\theta = 180°$.

Research Reports

No.	Authors	Title
98-09	M.J. Grote	Nonreflecting Boundary Conditions For Electromagnetic Scattering
98-08	M.J. Grote, J.B. Keller	Exact Nonreflecting Boundary Condition For Elastic Waves
98-07	C. Lage	Concept Oriented Design of Numerical Software
98-06	N.P. Hancke, J.M. Melenk, C. Schwab	A Spectral Galerkin Method for Hydrodynamic Stability Problems
98-05	J. Waldvogel	Long-Term Evolution of Coorbital Motion
98-04	R. Sperb	An alternative to Ewald sums, Part 2: The Coulomb potential in a periodic system
98-03	R. Sperb	The Coulomb energy for dense periodic systems
98-02	J.M. Melenk	On n-widths for Elliptic Problems
98-01	M. Feistauer, C. Schwab	Coupling of an Interior Navier–Stokes Problem with an Exterior Oseen Problem
97-20	R.L. Actis, B.A. Szabo, C. Schwab	Hierarchic Models for Laminated Plates and Shells
97-19	C. Schwab, M. Suri	Mixed *hp* Finite Element Methods for Stokes and Non-Newtonian Flow
97-18	K. Gerdes, D. Schötzau	*hp* FEM for incompressible fluid flow - stable and stabilized
97-17	L. Demkowicz, K. Gerdes, C. Schwab, A. Bajer, T. Walsh	HP90: A general & flexible Fortran 90 *hp*-FE code
97-16	R. Jeltsch, P. Klingenstein	Error Estimators for the Position of Discontinuities in Hyperbolic Conservation Laws with Source Terms which are solved using Operator Splitting
97-15	C. Lage, C. Schwab	Wavelet Galerkin Algorithms for Boundary Integral Equations
97-14	D. Schötzau, C. Schwab, R. Stenberg	Mixed *hp* - FEM on anisotropic meshes II: Hanging nodes and tensor products of boundary layer meshes
97-13	J. Maurer	The Method of Transport for mixed hyperbolic - parabolic systems
97-12	M. Fey, R. Jeltsch, J. Maurer, A.-T. Morel	The method of transport for nonlinear systems of hyperbolic conservation laws in several space dimensions
97-11	K. Gerdes	A summary of infinite element formulations for exterior Helmholtz problems